1
2
3
4
5
6
7
8
9
10
11
12
13
14
15
16
17
18
19
20
21
22
23
24
25
26
27
28
29
30
31
32
33
34
35
36
37
38
39
40
41
42
43
44
45
46
47
48
49
50
51
52
53
54
55
56
57
58
59
60

3D Coincidence Imaging Disentangles Intense Field

Double Detachment of SF_6^-

Kandhasamy Durai Murugan, Yishai Albeck, Krishna Jagtap, Daniel Strasser

Institute of Chemistry, The Hebrew University of Jerusalem, 91904 Jerusalem, Israel.

Corresponding Author

* Daniel Strasser. Institute of Chemistry, The Hebrew University of Jerusalem, Jerusalem-91904,

Israel.   Email: strasser@huji.ac.il

ABSTRACT

The efficient intense field double detachment of molecular anions observed in SF_6^- is studied by 3D coincidence imaging of the dissociation products. By disentangling specific product channels, the dissociation anisotropy and kinetic energy release distributions are determined for the SF_5^+ + F fragmentation products, corresponding to the energetically lowest double detachment channel. The observed nearly isotropic dissociation with respect to the linear laser polarization and surprisingly high kinetic energy release events suggest that the dissociation occurs on a highly excited state. Rydberg (SF_6^+)* states composed of a highly repulsive dication core and a Rydberg electron are proposed to explain the observed kinetic energy release, accounting also for the efficient production of all possible cationic fragments at equivalent laser intensities.

KEYWORDS

Coincidence imaging, Intense field, Double detachment, Kinetic Energy Release, Rydberg states, Photoionization

INTRODUCTION:

Interaction of intense laser pulses with atoms and molecules induces a variety of dynamical processes. [1-4] Phenomena studied over the last years include molecular alignment,[1, 4] multi-photon ionization,[1-3] above threshold ionization,[1-3, 5] double ionization,[3,5-6] frustrated tunnel-ionization,[7] Coulomb explosion[1,5] and high order harmonic generation (HHG).[8-12] One of the major achievements in the field was the development of an intuitive rescattering mechanism picture, in which the first electron released is accelerated and rescattered from its parent system by the oscillating intense laser field to recombine and emit HHG photons or efficiently release a second electron.[8] Accordingly, the rescattering mechanism is extremely sensitive to laser polarization accounting for the acute suppression of HHG by polarization ellipticity.[12-14] This intuitive description of intense field interaction with atoms and molecules opened new pathways for using the HHG process itself as a spectroscopic tool and for probing light matter interaction on the attosecond time scale.[15-18] Furthermore, based on the rescattering model, bi-chromatic counter-rotating circularly-polarized laser pulses were specially designed and implemented to produce circularly polarized HHG pulses.[14] So far, the majority of experimental and theoretical efforts to understand the interaction of intense laser pulses with matter were performed on overall neutral atomic and molecular systems.[1-7,19-22] Significant efforts were invested also in studies of cationic systems that are inherently important for describing mechanisms involving early ionization of the neutral species by the intense laser pulse.[23-27] Intense field interactions with anions are intrinsically different from both neutral and cationic systems. The typically low electron detachment energies of anions make it possible to realize extreme conditions of very rapid detachment at relatively low laser intensities. In addition, using anions allows significantly higher contrast between the low energy required to remove the first electron and high ionization

potential energy required to remove the second electron. Furthermore, rescattering dynamics in anionic systems fundamentally differs from those in overall neutral systems due to the absence of the attractive Coulomb potential acting in rescattering process.[28-29] Nevertheless, partly due to the experimental challenges, intense field interaction with molecular anions received relatively lower attention, primarily concentrated on the photoelectron spectroscopy of atomic and simple diatomic anion systems.[29-37] Theoretical modeling of the F^- multi-photon detachment photoelectron spectrum demonstrate the importance of electron correlation effects and the possible contribution of rescattering dynamics.[36-37] Based on increased rates for linear versus circular laser polarizations Pedregosa-Gutierrez *et al.* reported evidence for a non sequential rescattering mechanism in intense field double detachment of atomic F^-.[29] On the other hand, we recently reported efficient multiple detachment of molecular SF_6^- anions exhibiting weak dependence on laser polarization that excludes the possibility of a semiclassical rescattering type mechanism.[38] As the parent SF_6^+ cation is not found, SF_n^+ fragments, as well as high lying dissociation channels leading to atomic S^+ and F^+ products are observed.[38] Similar to intense field double ionization in atomic and neutral species, the double detachment mechanism was found to be non-sequential based on laser pulse shaping experiments.[30] One of the surprising observations is that cation fragments that are known to have very different appearance energies (AE) in the dissociative ionization of neutral SF_6 appear and also reach saturation at equivalent laser intensities leading to multiple detachment of the SF_6^- anion.[38] For example, SF_5^+ is the lowest AE dissociation product of the unstable SF_6^+ ground state with AE of 15.3 eV above the neutral SF_6 system.[39] In contrast, the atomic F^+ product has a higher 38 eV AE.[40] The energetic difference of 22.7 eV between the two products corresponds to absorption of almost 15 photons of 800 nm wavelength, nevertheless, both SF_5^+ and F^+ products of intense field double

detachment of SF_6^- are observed to appear at peak intensities as low as $\sim 5 \times 10^{13}$ W/cm^2.[41] For neutral SF_6, SF_5^+ and F^+ products of multiple ionization are observed at one – two orders of magnitude higher laser peak intensities.[42-43] In view of the pivotal role of early work on intense field double ionization of neutral systems, leading to the development of attosecond technology,[8] it is attractive to further explore the dominant mechanisms controlling intense field interactions with strongly correlated multi-electron systems such as molecular anions.

In this paper we use 3D coincidence imaging of the correlated fragments from a single SF_6^- molecule at a time to disentangle the different competing double detachment channels. Most importantly double detachment of SF_6^- leading to dissociative ionization channels are clearly resolved from cations produced in multiple ionization followed by Coulomb explosion. Channel-specific dissociation velocity distribution in the molecular frame of reference and corresponding kinetic energy release (KER) are obtained. The role of highly excited $(SF_6^+)^*$ cation states in the double detachment mechanism is discussed in view of the observed high KER events in the lowest AE channel of $SF_5^+ + F$, shedding light on the efficient production of SF_5^+ and F^+ products at equivalent, relatively low, peak intensities.

EXPERIMENTAL SETUP:

The experimental apparatus was previously described in detail.[38, 41] Briefly, cold SF_6^- anions are formed by electron capture in a supersonic expansion of Argon carrier gas seeded with $\sim 1\%$ SF_6 sample.[44] After the expansion, ions are accelerated up to $E_0 \sim 4.8$ keV kinetic energy in a pulsed Wiley−McLaren type mass spectrometer[45] directing the ion beam pulse towards the photofragment spectrometer shown schematically in figure-1. Based on their time of flight, ions of selected charge over mass ratio are allowed to continue into the spectrometer, while ions arriving at different times are deflected by $\pm$ 750V potentials applied to the upper and lower

electrodes of the mass gate deflector. Selected SF_6^- ions are further accelerated by the spectrometer potential (U_{SP} ~3.1 keV) before arriving to the field-free laser−ion interaction region. In the interaction region the ion beam is intersected by the optical path of a focused intense 800nm laser beam. The peak intensity reached by the ~3mJ and 35fs laser pulse is computer controlled by displacement of a 250mm focal length lens, reaching up to ~3×10^{15} W/cm^2 at the focal spot.
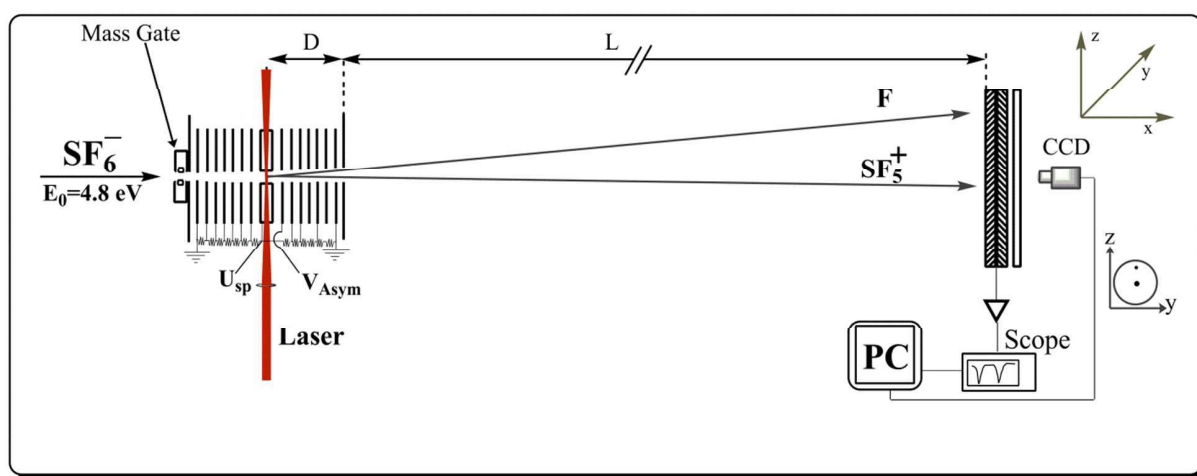

Figure-1: Schematic representation of experimental set-up. Mass selected SF_6^- ions interact with a focused intense fs laser pulse at the photofragment spectrometer ion-laser interaction region. The fragments are mass resolved by the U_{sp} photofragment spectrometer potential and detected in coincidence on a time and position sensitive detector located downstream of the photofragment spectrometer.

As the desired photofragmentation events occur in the moving frame of the anion beam, all fragments continue towards the time and position sensitive micro-channel plate (MCP) detector located downstream of the photofragment spectrometer. The initial velocity of the parent anion molecule, corresponding to an E_0+U_{sp} kinetic energy, provides sufficient energy for detection of all the charged as well as neutral photofragments that are separated according to their charge over mass ratios by the spectrometer potential, U_{sp}. Cationic photofragments are accelerated, reaching the detector first, followed by the neutral products of laser-ion interaction while the

parent anion beam as well as negatively charged fragments are decelerated arriving last to the detector. In this way all cationic and neutral photoproducts can be efficiently detected.

For each laser pulse, the time and position of the correlated fragment hits on the MCP detector surface are acquired by a computer. The electronic timing signal from the MCP detector is digitized using a fast scope,[46] while the 2D position information is read out optically from the P46 phosphor anode by a high frame rate CCD camera.[47] Both CCD exposure and scope acquisition times are synchronized to the laser pulse to record only cationic and neutral products, while detection of the parent anion beam arriving to the detector at later times is avoided in order to suppress random coincidences. Fast peak finding routines are implemented to extract the times of flight and pulse amplitudes from the electronic signal, as well as the 2D positions and brightness of the coincident optical signals.

Figure-2 shows a typical photofragment time of flight (TOF) coincidence map, allowing clear identification of fragmentation events as specific final channels. For example, the dotted contour (a) in figure-2 marks events in which a SF_5^+ product is detected in coincidence with a neutral fragment, corresponding to the lowest AE cation fragmentation channel producing $SF_5^+ + F$. Particle hit positions are assigned with charge over mass ratios according to the correlation between the brightness of optically collected position signals and amplitude of the electronic timing signals to take advantage of the high statistical variance of MCP detector gain in order to correlate coincident time and position information for each dissociation event. The good correlation of electronic timing signal amplitudes and the corresponding optical position signal brightness in our setup is demonstrated in figure-3. Thus, considering two randomly selected fragment hits and assigning the high and low amplitude hits to the respectively high and low brightness peaks, we estimate less than 5% assignment error probability for two-hit events.

Similar approaches for 3D coincidence imaging of multi-particle fragmentation events by correlating brightness and amplitude of MCP detectors were recently developed and described in detail.[48-49]
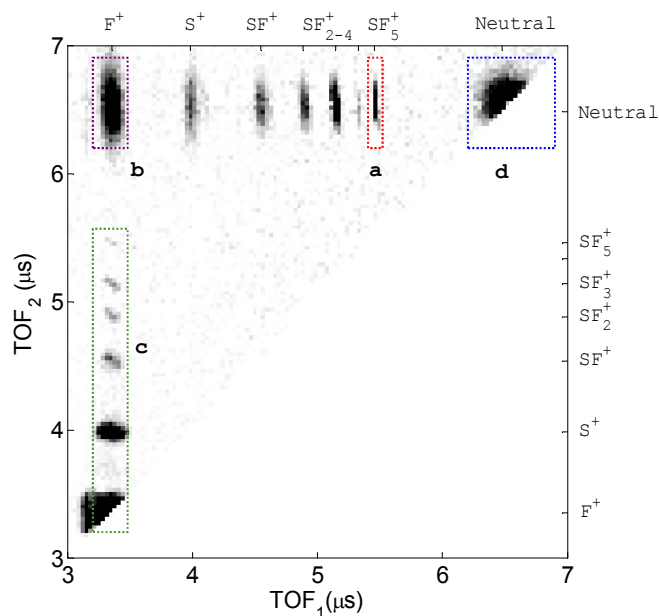

Figure-2: Two-fragment TOF coincidence map for intense field multiple detachment of SF_6^-. The doted contours mark coincidence events selected for the 'Z-scan' analysis. Contour (a) corresponds to $SF_5^+ + F$ coincidence events, (b) corresponds to $F^+ +$ neutral coincidence, (c) corresponds to $F^+ +$ cation coincidence and neutral-neutral coincidence are marked by contour (d).

Based on this assignment of optically measured positions to their respective times of flight, 3D velocities of the detected fragments are calculated in the molecular frame of reference. The V_y and V_z velocities in the 2D detector plane are calculated for each fragment by dividing fragment position displacements from the center of mass by the respective TOFs. The respective V_x dissociation velocities along the TOF axis are calculated by taking into account the fragment charge over mass ratio, TOF, parent ion velocity and the acceleration of cationic fragments by the exact position dependent photofragment spectrometer potential calculated using SIMION

simulation.[50] Finally, the center of mass momentum of the correlated fragments for each

fragmentation event is calculated and compared to the parent anion beam momentum spread,

allowing rejection of partial detection or accidental erroneous assignment of times of flight to the

2D positions in the detector plane. Thus, 3D coincidence imaging enables the observed products,

the kinetic energy release, and fragment orientation distributions corresponding to a specific final

channel to be extracted.
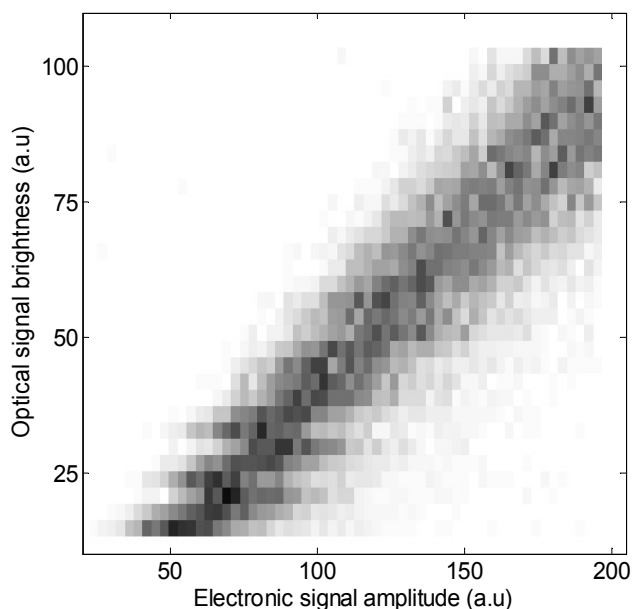
Figure-3: Correlation between the optical signal brightness and electronic signal amplitudes. For
higher signal levels a non-linear correlation can be observed due to the larger spot
size of the 2D position signal (not shown).

In the relatively simple case of SF_5^+ + neutral coincidence, the neutral product assignment as a F

atom is unambiguous. On the other hand, due to the finite MCP detection efficiency, neutral

fragments detected in coincidence with smaller cation fragments could be indeed due to 2-body

fragmentation or due to partially detected 3 body and even 4-body fragmentation channels. For

example, analysis of the center of mass momentum for the correlated F^+ and neutral fragments

clearly indicates that these events, marked by the dotted contour (b) in figure-2, cannot be assigned to the $SF_5 + F^+$ fragmentation channel and must involve higher degree of fragmentation. It is important to note that even in the simple $SF_5^+ + F$ case, coincidence detection is vital for exclusion of events with higher ionization levels such as $SF_5^+ + F^+$ Coulomb explosion channel that can be expected to exhibit utterly different fragmentation dynamics.[38]
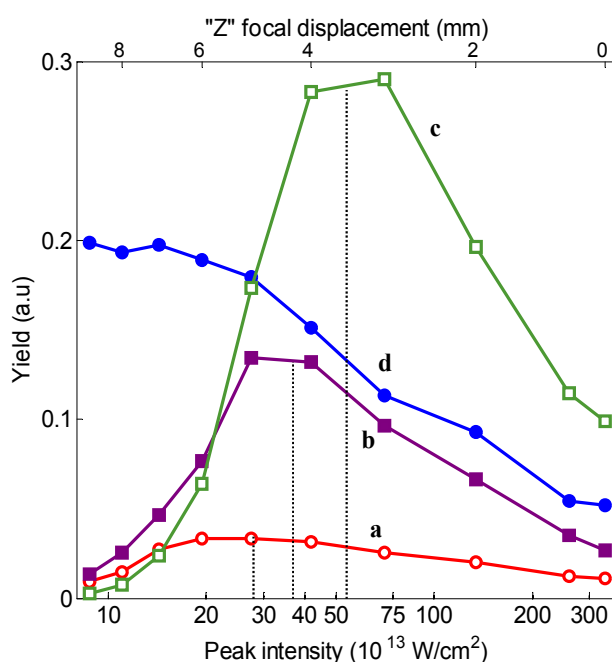
RESULTS AND DISCUSSION:

Figure-4: 'Z-scan' analysis shows yield of selected coincidence events as a function of peak intensity, varied by displacing the laser focal point with linearly polarized laser pulse. (a) $SF_5^+ + F$ coincidence (open circle), (b) $F^+ +$ neutral coincidence (full square), (c) $F^+ +$ cation coincidence (open square) and (d) neutral-neutral coincidence event rates (full circle). Maximal yields for coincidence channels (a-c) are observed at focal displacements corresponding to 28 ± 6, 37 ± 10 and $54\pm17 \times10^{13}$ W/cm^2 peak intensities.

Figure-4 presents a "Z-scan" analysis[41] of different coincidence event yields as a function of laser focal point displacement from the anion target and the corresponding peak intensity at the ion-laser interaction region. For each type of coincidence event, the maximal yield is obtained at

a "Z" displacement balancing the non-linear dependence of rate on peak intensity and the vanishing interaction volume approaching the focal point. The corresponding peak intensity is directly related to the saturation intensity of the specific non-linear process by a geometric factor of ~3.0, considering a Gaussian beam profile and an *a-priori* unknown nonlinear intensity dependence.[41] Thus, a $9\pm2\times10^{13}$ W/cm^2 saturation intensity is determined for the $SF_5^+ + F$ channel, F$^+$ yield in coincidence with neutral products saturates at a comparable $12\pm4\times10^{13}$ W/cm^2 peak intensity and cation-cation coincidence events are found to saturate at $18\pm6\times10^{13}$ W/cm^2. Although the saturation intensities reported here are in agreement with the respective saturation of the total molecular and atomic singly charged cation yields reported in reference[41], we note a small systematic correction towards lower intensities. This correction reflects our ability to resolve coincidence events and not only charge over mass, allowing cation-neutral events to be disentangled from higher ionization channels which produce cation-cation and cation-dication coincidences that saturate at higher intensities.
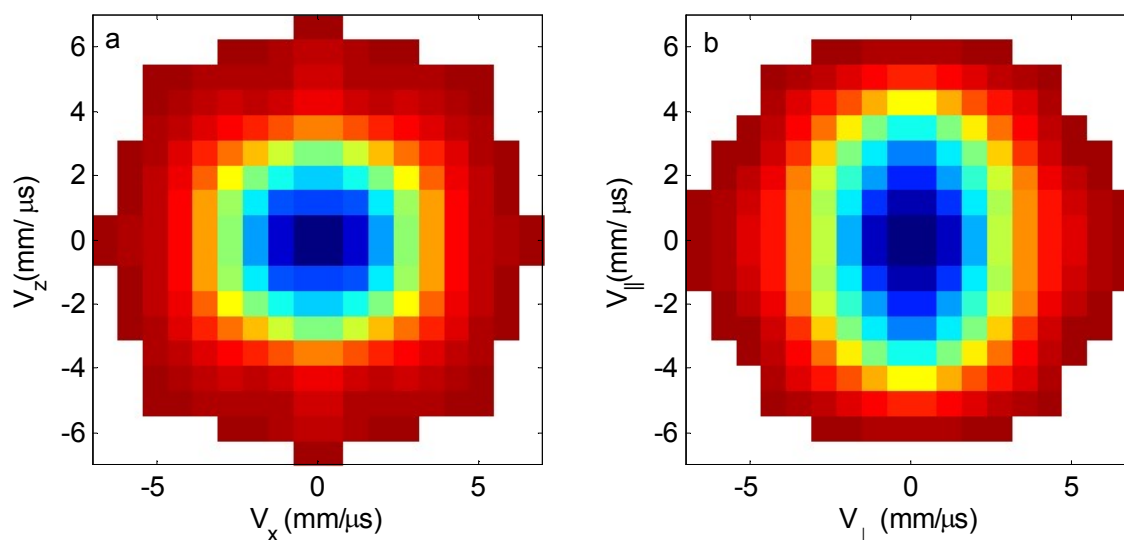
Figure-5: a) Probability distribution $P(V_x, V_z)$ of velocity components for the $SF_5^+ + F$ fragmentation channel in the plane perpendicular to the laser polarization; where V_x derived from TOF information and V_z derived from axis parallel to the laser propagation axis. b) probability distribution $P(V_\parallel, V_\perp)$ of velocity component parallel and perpendicular to the axis of laser polarization.

Figures-5a and 5b show projected 3D dissociation velocity distributions recorded for the SF_5^+ + F final channel events. Figure-5a shows the $P(V_x, V_z)$ distribution in the plane perpendicular to the laser polarization. The data shown in figure 5a and 5b are symmetrized with respect to reflection about both X and Z axes. Although one can expect symmetry under rotation in the XZ plane, the data is not symmetrized by rotation as V_x is derived from the time of flight measurement, while V_z is derived from the position displacements in the detector plane. The rather symmetric velocity distribution shown in figure-5a is therefore indicative of a successful conversion of timing and position data to 3D dissociation velocities in the molecular frame of reference.

Figure-5b shows the $P(V_{\parallel}, V_{\perp})$ probability distribution of the velocity component parallel and perpendicular to the linear laser polarization along the Y-axis. Typical intense field processes driven with linearly polarized light exhibit high degree of anisotropy, as the angular momentum of many photons has to be conserved.[6, 21, 51] Nevertheless, the dissociation velocity distribution is found to be rather isotropic, with only a small preference to fragmentation parallel to laser polarization characterized by a low β-parameter of ~0.4±0.2. Isotropic emission may seem consistent with the high O_h symmetry of neutral SF_6, however, the SF_6^- anion is expected to have a lower C_{4v} symmetry.[52] Furthermore, dissociative photoionization of the neutral SF_6 using photon energies up to 28 eV exhibits significantly higher alignment of the SF_5^+ fragments characterized by β-parameter of 1-1.3 with respect the light polarization axis.[53] The anisotropic dissociative ionization was assigned to the $6a_{1g}$ and $6t_{1u}$ superexcited SF_6 states that dominate the SF_6 photoionization mechanism in the 20-35 eV photon energy range.[54] The observed nearly isotropic emission can be consistent with photoionization at higher photon energies, as photoion emission anisotropy was reported to gradually vanish between 40 and 100 eV photon energies.[54]

On the other hand, the lack of alignment at higher photon energies was attributed to new channels producing isotropic fragmentation, leading also to higher AE fragments.[54-55] It is important to note that delayed fragmentation on the rotational timescale can also lead to loss of alignment due to molecular rotational depolarization.[56] However, even ground state SF_6^+ fragmentation is expected to proceed rapidly on the femtosecond timescale.[57] It is therefore reasonable to assume that the observed angular distribution reflects the dissociation axis angle with respect to the laser polarization.
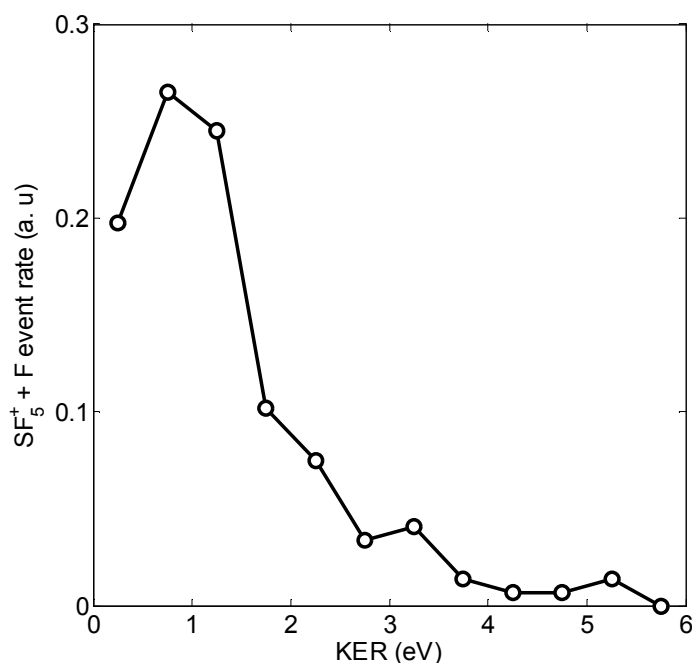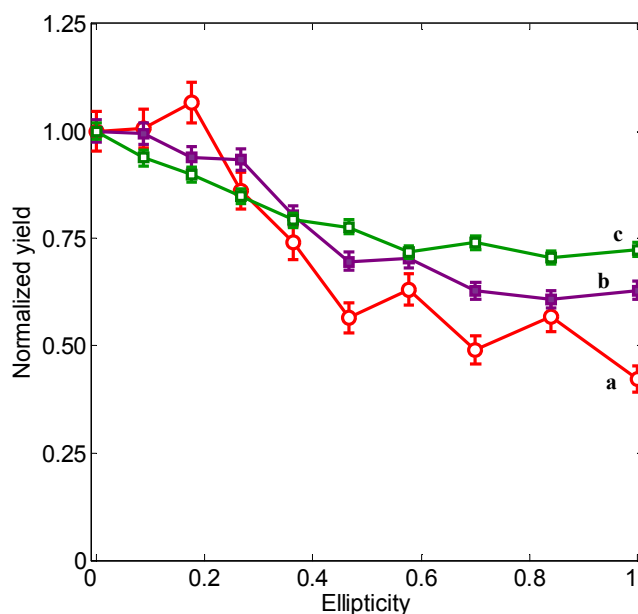

Figure-6: Total Kinetic energy release distribution for the SF_5^+ + F channel.

Three dimensional coincidence imaging data also allows us to derive the total kinetic energy release in each fragmentation event. Figure-6 shows the measured KER distribution for the SF_5^+ + F final channel. The average KER observed is ~1.3 eV, with 80% of the dissociation events observed with KER below 2 eV. The remaining 20% of the events exhibit a tail of the KER distribution towards high KER values up to ~5 eV. Dissociative photoionization of neutral SF_6

typically leads to ~0.12 eV observed for SF_5^+ cation products, inferring typical total KER of ~1 eV and up to ~1.5 eV.[53, 58-59] Even photoionization with higher energy photons leads to less than 1.5 eV KER in the dissociation of SF_6^+.[53] The observed high KER events above 1.5 eV in the SF_5^+ + F dissociative double detachment channel are therefore surprising. High KER events, as those shown in figure-6, are typically observed in multiple ionization of SF_6 followed by dissociation of the SF_6^{2+} dication, e.g. fragmenting into correlated SF_5^+ and F^+ fragments.[60] The Coulomb repulsion of the two cations at close proximity leads to high KER, reaching up to 5.8 eV observed for the SF_5^+ + F^+ Coulomb explosion following $3t_{1u}$ inner shell ionization with a 2MeV ion beam.[59] The pure Coulombic energy contribution to the KER scales with one over the initial cation-cation distance at the instance of double ionization. One can therefore speculate that Coulomb explosion initiated from SF_6^- would result in lower KER based on the elongation of the equilibrium S-F bond length from 1.56 Å in neutral SF_6 to 1.73 Å in the anion system.[52, 61] Sanderson *et al.* observed F^+ and SF_5^+ products in time of flight mass spectroscopy of neutral SF_6 molecules ionized by intense laser pulses and tentatively attributed high KER products at peak intensities above 10^{15} W/cm^2 to the formation of multiply ionized SF_6^{q+} undergoing coulomb explosion and low KER fragments at ~4.3×10^{14} W/cm^2 to dissociative ionization.[42] However, with the advent of neutral detection capability and 3D coincidence imaging these competing final channels are disentangled such that only SF_5^++ neutral F atom events and no SF_5^+ + F^+ Coulomb explosion events contribute to the KER distribution shown in figure 6. The observed high KER events without Coulomb explosion can be explained by dissociation on high-lying Rydberg $(SF_6^+)^*$ states, composed of a SF_6^{2+} dication core leading to a highly repulsive potential and a loosely bound Rydberg electron.[8, 62-63] Such Rydberg state mechanism was previously proposed for explaining high KER neutral fragment production in intense field dissociation of the D_3^+

molecular cation by Frustrated tunnel ionization (FTI) .[62-63] FTI leading to producing high lying

Rydberg states, was also reported for intense field interaction with neutral atomic systems,

leading even to an observable deflection of neutral atoms by the intense laser field.[64]

Figure-7: Ellipticity scan profile corresponding to (a) $SF_5^+ + F$ coincidence (open circle), (b) F^+ + neutral coincidence (full square), (c) F^+ + cation coincidence (open circle) events.

Previous work on neutral and cationic systems propose a rescattering based FTI

mechanism.[58-59] On the other hand, figure-7 shows the channel-specific coincidence event yields

weak dependence on the laser polarization ellipticity. These channel-specific data confirm the

conclusion reached based on the integrated measurement in reference[38] namely that the dominant

double detachment mechanism observed here is inconsistent with a semi-classical rescattering

mechanism which is critically quenched by ellipticity.[12-13] Similarly, the non-sequential nature of

the double detachment process is confirmed for the channel-specific yields that are observed to

be suppressed by pre-pulses compared to post-pulses, respectively introduced by negative and

positive third order dispersion (TOD) pulse shaping.[38] It was recently demonstrated that elliptical

HHG in molecular systems using elliptical pulses can be observed via favorable resonances of the neutral system, beyond the simple rescattering picture.[65,66] Therefore, although inconsistent with a typical response of rescattering mechanism to polarization ellipticity we propose that the non-sequential nature of SF_6^- double detachment could support frustrated ionization, producing highly repulsive Rydberg states leading to $SF_5^+ + F$ channel.

CONCLUSION:

The combined evidence of high KER events characteristic of SF_6^{2+} coulomb explosion and nearly isotropic dissociation indicate that even the lowest double detachment channel is reached via highly excited SF_6^+ cation states rather than the shape resonance states that dominate the photoionization threshold of SF_6.[53] The high KER, characteristic of Coulomb explosion of a SF_6^{2+} dication, suggests involvement of $(SF_6^+)^*$ Rydberg states with a SF_6^{2+} dication core and a Rydberg electron, similar to high lying Rydberg states observed in FTI of neutral and cationic systems.[62-64] Such high excitation in the double detachment process can explain the efficient production of all possible cation fragments at equivalent laser peak intensities. For example, the rapid dissociation on the high-lying state can asymptotically lead the Rydberg electron either to the F^* atom or to the SF_5^*. Thus, accounting also for the unexpected equivalently efficient production of F^+ and SF_5^+, observed for peak intensities near the double detachment threshold despite the ~23 eV AE difference of the molecular and atomic cation fragments. Subsequent fragmentation of the excited SF_5^* neutral product would be in agreement with our observation that neutrals detected in coincidence with F^+ are inconsistent with SF_5, based on center of mass momentum conservation. Further theoretical work is needed to explain how the highly dissociative states are formed in the non-sequential and double detachment of molecular anions such as SF_6^-.

AUTHOR INFORMATION

Corresponding Author

*Email: strasser@huji.ac.il

Notes

The authors declare no competing financial interests.

ACKNOWLEDGMENT

REFERENCES

(1) Posthumus, J. H. The Dynamics of Small Molecules in Intense Laser Fields. *Rep. Prog. Phys.* **2004**. *67*, 623–665.

(2) Protopapas, M.; Keitel, C. H.; Knight, P. L. Atomic Physics with Super-High Intensity Lasers. *Rep. Prog. Phys.* **1997**, *60*, 389–486.

(3) Joachain, C. J.; Kylstra, N. J.; Potvliege, R. M. *Atoms in intense laser fields*; Cambridge University Press: Cambridge, U. K.; 2012**.**

(4) Stapelfeldt, H.; Seideman, T. Aligning Molecules with Strong Laser Pulses. *Rev. Mod. Phys.* **2003**, *75*, 543–557.

(5) Sheehy, B. Chemical Processes in Intense Optical Fields. *Ann. Rep. Prog. Chem. Sect. C*, **2001**, *97*, 383–410.

(6) Weber, Th.; Weckenbrock, M.; Staudte, A.; Spielberger, L.; Jagutzki, O.; Mergel, V.; Afaneh, F.; Urbasch, G.; Vollmer, M.; Giessen, H. *et al*. Recoil-Ion Momentum Distributions for Single and Double Ionization of Helium in Strong Laser Fields. *Phys. Rev. Lett.* **2000**, *84*, 443−446.

(7) Nubbemeyer, T.; Gorling, K.; Saenz, A.; Eichmann, U.; Sandner, W. Strong-Field Tunneling without Ionization. *Phys. Rev. Lett*. **2008**, *101*, 233001.

(8) Corkum, P. B. Plasma Perspective on Strong-Field Multiphoton Ionization. *Phys. Rev. Lett.* **1993**, *71*, 1994−1997.

(9) Paul, P. M.; Toma, E. S.; Breger, P.; Mullot, G.; Auge, F.; Balcou, Ph.; Muller, H. G.; Agostini, P. Observation of a Train of Attosecond Pulses from High Harmonic Generation. *Science* 2001, *292*, 1689−1692.

(10) Seres, J.; Seres, E.; Verhoef, A. J.; Tempea, G.; Strelill, C.; Wobrauschek, P.; Yakovlev, V.; Scrinzi, A.; Spielmann, C.; Krausz, F. Source of Coherent Kiloelectronvolt X-rays. *Nature* 2005, *433*, 596.

(11) L'Huillier, A.; Schafer, K. J.; Kulander, K. C. Theoretical Aspects of Intense Field Harmonic Generation. *J. Phys. B: At. Mol. Opt. Phys.* **1991**, *24*, 3315–3341.

(12) Dietrich, P.; Burnett, N. H.; Ivanov, M.; Corkum, P. B. High- Harmonic Generation and Correlated Two-Electron Multiphoton Ionization with Elliptically Polarized Light. *Phys. Rev. A*. **1994**, *50*, 3585−3588.

(13) Budil, K. S.; Salières, P.; Perry, M. D.; L'Huillier, A. Influence of Ellipticity on Harmonic Generation. *Phys. Rev. A*, **1993**, *48*, 3437–3440.

(14) Kfir, O.; Grychtol, P.; Turgut, E.; Knut, R.; Zusin, D.; Popmintchev, D.; Popmintchev, T.; Nembach, Shaw, J. M.; Fleischer, A. *et al*. Generation of Bright Phase-Matched Circularly-Polarized Extreme Ultraviolet High Harmonics *Nature. Photon*. **2015**, *9*, 99–105

(15) Corkum, P. B.; Krausz, F. Attosecond Science. *Nature. Phys.* **2007**, *3*, 381–387.

(16) Krausz, F.; Ivanov, M. Attosecond Physics. *Rev. Mod. Phys*. **2009**. *81*, 163–234.

(17) Itatani, J.; Levesque, J.; Zeidler, D.; Niikura, H.; Pepin, H.; Kieffer, J. C.; Corkum, P. B.; Villeneuve, D. M. Tomographic Imaging of Molecular Orbitals. *Nature*. **2004**, *432*, 867–871.

(18) Shafir, D.; Soifer, H.; Bruner, B. D.; Dagan, M.; Mairesse, Y.; Patchkovskii, S.; Ivanov, M.Y.; Smirnova, O.; Dudovich, N. Resolving the Time When an Electron Exits a Tunnelling Barrier. *Nature*. **2012**, *485*, 343–346.

(19) Codling, K.; Frasinski, L. J. Dissociative Ionization of Small Molecules in Intense Laser Fields. *J. Phys. B: At. Mol. Opt. Phys.* **1993**, *26*, 783–809.

(20) Akagi, H.; Otobe, T.; Staudte, A.; Shiner, A.; Turner, F.; Dörner, R.; Villeneuve, D. M.; Corkum, P. B. Laser Tunnel Ionization from Multiple Orbitals in HCl. *Science.* **2009**, *325*, 1364–1367.

(21) Holmegaard, L.; Hansen, J. L.; Kalhøj, L.; Louise Kragh, S.; Stapelfeldt, H.; Filsinger, F.; Küpper, J.; Meijer, G.; Dimitrovski, D.; Abu-samha, M. *et al*. Photoelectron Angular Distributions from Strong-Field Ionization of Oriented Molecules. *Nature. Phys*, **2010**, *6*, 428–432.

(22) Rudenko, A.; Zrost, K.; Feuerstein, B.; de Jesus, V. L. B.; Schröter, C. D.; Moshammer, R.; Ullrich, J. Correlated Multielectron Dynamics in Ultrafast Laser Pulse Interactions with Atoms. *Phys. Rev. Lett*. **2004**, *93*, 253001.

(23) Prabhudesai, V. S.; Lev, U.; Natan, A.; Bruner, B. D.; Diner, A.; Heber, O.; Strasser, D.; Schwalm, D.; Ben-Itzhak, I.; Hua, J. J. *et al*. Tracing the Photodissociation Probability of H_2^+ in Intense Fields using Chirped Laser Pulses. *Phys. Rev. A.* **2010**, *81*, 023401.

(24) Zohrabi, M.; McKenna, J.; Gaire, B.; Johnson, N. G.; Carnes, K. D.; De, S.; Bocharova, I.A.; Magrakvelidze, M.; Ray, D.; Litvinyuk, I. V. *et al*. Vibrationally Resolved Structure in O_2^+ Dissociation Induced by Intense Ultrashort Laser Pulses. *Phys. Rev. A.* **2011**, *83*, 053405.

(25) Benis, E. P.; Bakarezos, M.; Papadogiannis, N. A.; Tatarakis, M.; Divanis, S.; Ó Broin, C.; Nikolopoulos, L. A. A. Role of Broadband-Laser-Pulse Temporal Extent in H_2^+ Photodissociation. *Phys. Rev. A.* **2012**, *86*, 043428

(26) Ben-Itzhak, I.; Wang, P. Q.; Sayler, A. M.; Carnes, K. D.; Leonard, M.; Esry, B. D.; Alnaser, A.; Ulrich, B.; Tong, X.; Litvinyuk, I. *et al*. Elusive Enhanced Ionization Structure for H_2^+ in Intense Ultrashort Laser Pulses. *Phys. Rev. A.* **2008**, *78*, 063419.

(27) Natan, A.; Lev, U.; Prabhudesai, V. S.; Bruner, B. D.; Strasser, D.; Schwalm, D.; Ben-Itzhak, I.; Heber, O.; Zajfman, D.; Silberberg, Y. Quantum Control of Photodissociation by Manipulation of Bond Softening. *Phys. Rev. A.* **2012**, *86*, 043418.

(28) Bhardwaj, V.; Aseyev, S.; Mehendale, M.; Yudin, G.; Villeneuve, D.; Rayner, D.; Ivanov, M.; Corkum, P. Few Cycle Dynamics of Multiphoton Double Ionization. *Phys. Rev. Lett.* **2001**, *86*, 3522–3525.

(29) Pedregosa-Gutierrez, J.; Orr, P.; Greenwood, J.; Murphy, A.; Costello, J.; Zrost, K.; Ergler, T.; Moshammer, R.; Ullrich, J. Evidence for Rescattering in Intense, Femtosecond Laser Interactions with a Negative Ion. *Phys. Rev. Lett.* **2004**, *93*, 223001.

(30) Greenwood, J. B.; Collins, G. F.; Pedregosa-Gutierrez, J.; McKenna, J.; Murphy, A.; Costello, J. T. Double Ionization of Atomic Negative Ions in an Intense Laser Field. *J. Phys. B: At. Mol. Opt. Phys.* **2003**, *36*, L235–L240.

(31) Kiyan, I.; Helm, H. Production of Energetic Electrons in the Process of Photodetachment of F^-. *Phys. Rev. Lett.* **2003**, *90*, 183001.

(32) Shearer, S. F. C.; Monteith, M. R. Direct Photodetachment of F^- by Mid-Infrared Few-Cycle Femtosecond Laser Pulses. *Phys. Rev. A*. **2013**, *88*, 033415.

(33) Gazibegović-Busuladžić, A.; Milošević, D. B.; Becker, W.; Bergues, B.; Hultgren, H.; Kiyan, I. Y. Electron Rescattering in Above-Threshold Photodetachment of Negative Ions. *Phys. Rev. Lett.* **2010**, *104*, 103004.

(34) Reichle, R.; Helm, H.; Yu. Kiyan, I. Detailed Comparison of Theory and Experiment of Strong-Field Photodetachment of the Negative Hydrogen Ion. *Phys. Rev. A.* **2003**, *68*, 063404.

(35) Hultgren, H.; Kiyan, I. Y. Photodetachment Dynamics of F_2^- in a Strong Laser Field. P*hys. Rev. A.* **2011**, *84*, 015401.

(36) van der Hart, H. W. Configuration-Interaction Effects in and Intensity Dependence of F^- Multiphoton Detachment. *J. Phys. B: At. Mol. Opt. Phys.* **2000,** *33*, 1789– 1803.

(37) Hassouneh, O.; Law, S.; Shearer, S. F. C.; Brown, A. C.; van der Hart, H. W. Electron Rescattering in Strong-Field Photodetachment of F^-. *Phys. Rev. A*. **2015**, *91*, 013422.

(38) Albeck, Y.; Kandhasamy, D. M.; Strasser, D. Multiple Detachment of the SF_6^- Molecular Anion with Shaped Intense Laser Pulses. *J. Phys. Chem. A*. **2014**, *118*, 388–395.

(39) Sasanuma, M.; Ishiguro, E.; Hayaisha, T.; Masuko, H.; Morioka, Y.; Nakajima, T.; Nakamura, M. Photoionisation of SF_6 in the XUV Region. *J. Phys. B: At. Mol. Opt. Phys.* **1979**, *12*, 4057−4063.

(40) Hitchcock, A.; Van der Wiel, M. J. Absolute Oscillator Strengths (5−63 eV) for Photoabsorption and Ionic Fragmentation of SF_6. *J. Phys. B: At. Mol. Opt. Phys.* **1979**, *12*, 2153−2169.

(41) Albeck, Y.; Kandhasamy, D. M.; Strasser, D. Z-Scan Method for Nonlinear Saturation Intensity Determination, Using Focused Intense Laser Beams. *Phys. Rev. A.* **2014**, *90*, 053422.

(42) Sanderson, J. H.; Thomas, R. V.; Bryan, W. A.; Newell, W. R.; Taday, P. F.; Langley, A. L. Multielectron-Dissociative-Ionization of SF_6 by Intense Femtosecond Laser Pulses. *J. Phys. B: At. Mol. Opt. Phys.* **1997**, *30*, 4499–4507.

(43) Ren, H.; Ma, R.; Li, X.; Chen, J.; Yang, H.; Gong, Q. Multielectron Dissociative Ionization of SF_6 in an Intense Femtosecond Laser Field. *Int. J. Mass Spectrom.* **2004,** *235*,117–122.

(44) Even, U.; Jortner, J.; Noy, D.; Lavie, N. Cooling of Large Molecules Below 1 K and He Clusters Formation. *J. Chem. Phys.* **2000**, *112*, 8068.

(45) Wiley, W. C.; McLaren, I. H. Time-of-Flight Mass Spectrometer with Improved Resolution. *Rev. Sci. Instrum.* **1955**, *26*, 1150.

(46) Picoscope 5203. Pico Technology Limited.

(47) Prosilica GE 680. Allied Vision Technologies Canada Inc.

(48) Urbain, X.; Bech, D.; Van Roy, J.-P.; Géléoc, M.; Weber, S.; Huetz, A.; Picard, Y. J. A Zero Dead-Time Multi-Particle Time and Position Sensitive Detector Based on Correlation Between Brightness and Amplitude. *Rev. Sci. Instrum.* **2015**, *86*, 023305.

(49) Lee, S. K.; Cudry, F.; Lin, Y. F.; Lingenfelter, S.; Winney, A. H.; Fan, L.; Li, W. Coincidence Ion Imaging with a Fast Frame Camera. *Rev. Sci. Instrum.* **2014**, *85*, 123303.

(50) SIMION: ion optics software, SIS, Inc.

(51) Hishikawa, A.; Liu, S.; Iwasaki, A.; Yamanouchi, K. Light-Induced Multiple Electronic-State Coupling of O_2^+ in Intense Laser Fields. *J. Chem. Phys.* **2001**, *114*, 9856.

(52) Eisfeld, W. Highly Accurate Determination of the Electron Affinity of SF_6 and Analysis of Structure and Photodetachment Spectrum of SF_6^-. *J. Chem. Phys*. **2011**, *134*, 054303.

(53) Peterka, D. S.; Ahmed, M.; Ng, C.; & Suits, A. G. Dissociative Photoionization Dynamics of SF_6 by Ion Imaging with Synchrotron Undulator Radiation. *Chem. Phys. Lett.* **1999**, *312*, 108–114.

(54) Ono, M.; Mitsuke, K. Anisotropy of Fragment Ions from SF_6 by Photoexcitation Between 23 and 210 eV. *Chem. Phys. Lett*. **2002**, *366*, 595–600.

(55) Ono, M.; Mitsuke, K. Kinetic Energy Distribution and Anisotropy of Fragment Ions from SF_6 by Photoexcitation of a Sulfur 2p-Electron. *Chem. Phys. Lett*. **2003**, *379*, 248–254.

(56) Buijsse, B.; van der Zande, W. Measurement of the Lifetime of Predissociative Diatomic Molecules. *Phys. Rev. Lett*. **1997**, *79*, 4558–4561.

(57) Tachikawa, H. The Ionization Dynamics of SF_6: A Full Dimensional Direct *Ab initio* Dynamics Study. *J. Phys. B: At. Mol. Opt. Phys*. **2000**, *33*, 1725–1733.

(58) Creasey, J. C.; Lambed, I. R.; Tuckett, R. P.; Codling, K.; Frasinski, L. J.; Hatherly, P. A.; Stankiewicz, M. Fragmentation of Valence Electronic States of SF_6^+ Studied with Synchrotron Radiation. *J. Chem. Soc. Faraday Trans*. **1991**, *87*, 1287–1292.

(59) Simm, I. G.; Danby, C. J.; Eland, J. H. D.; Mansell, P. I. Translational Energy Release in the Loss of Fluorine Atoms from the Ions SF_6^+, CF_4^+ and $C_2F_6^+$. *J. Chem. Soc., Faraday Trans. 2.* **1976**, *72*, 426–434.

(60) Lange, M.; Pfaff, O.; Muller, U. Projectile Fragment − Ion Fragment − Ion Coincidences PFIFICO Following Fast Ion Impact on SF_6. *Chem. Phys.* **1998**, *230*, 117–141.

(61) Tachikawa, H. *Ab initio* MO Calculations of Structures and Electronic States of SF_6 and SF_6^-. *J. Phys. B: At. Mol. Opt. Phys.* **2002**, *35*, 55–60.

(62) Li, M.; Qin, L.; Wu, C.; Peng, L.; Gong, Q.; Liu, Y. Rescattering and Frustrated Tunneling Ionization of Atoms in Circularly Polarized Laser Fields. *Phys. Rev. A.* **2014**, *89*, 013422.

(63) McKenna, J.; Sayler, A. M.; Gaire, B.; Kling, N. G.; Esry, B. D.; Carnes, K. D.; Ben-Itzhak, I. Frustrated Tunneling Ionization During Strong-Field Fragmentation of D_3^+. *New J. Phys.* **2012**, *14*, 103029.

(64) Eichmann, U.; Nubbemeyer, T.; Rottke, H.; Sandner, W. Acceleration of Neutral Atoms in Strong Short-Pulse Laser Fields. *Nature.* **2009**, *461*, 1261–1264.

(65) Ferré, A.; Handschin, C.; Dumergue, M.; Burgy, F.; Comby, A.; Descamps, D.; Fabre, B. Garcia, G. A. Géneaux, R. Merceron, L. *et al*. A Table-Top Ultrashort Light Source in the Extreme Ultraviolet for Circular Dichroism Experiments. *Nature Photon.* **2014**, *9*, 93–98.

(66) Ferré, A.; Boguslavskiy, A. E.; Dagan, M.; Blanchet, V.; Bruner, B. D.; Burgy, F.; Camper, A.; Descamps, D.; Fabre, B.; Fedorov, N. Multi-Channel Electronic and Vibrational Dynamics in Polyatomic Resonant High-Order Harmonic Generation. *Nat. Commun*. 2015, 6, 5952.

Table of Content

3D Coincidence Imaging Disentangles Intense Field Double Detachment of SF_6^-

Kandhasamy Durai Murugan, Yishai Albeck, Krishna Jagtap, Daniel Strasser